Supporting Information

Regulable high-contrast mechanofluorochromic enhancement behaviour based on substituent effects

Guang Yang,‡[a] Wen-Xuan Zhao,‡[a] Jing-Yi Cao,[a] Zeng-Min Xue,[a] Hong-Tao Lin,[a] Shu-Hai Chen,*[a] Takehiko Yamato,*[b] Carl Redshaw[c] and Chuan-Zeng Wang*[a]

Contents

Figure S16. Solvatochromism effect of absorption spectra for **2-PyBP** in Cyclohexane, 1, 4-Dioxane, THF, DCM and DMF, respectively.

Figure S17. Solvatochromism effect of absorption spectra for **1-BuPyBP** in Cyclohexane, 1, 4-Dioxane, THF, DCM and DMF, respectively.

Figure S18. Solvatochromism effect of absorption spectra for **2-BuPyBP** in Cyclohexane, 1, 4-Dioxane, THF, DCM and DMF, respectively.

Figure S19. Solvatochromism effect of emission spectra for **1-PyBP** in solvents with varying polarity (A) and CIE 1931 chromaticity diagram (B).

Figure S20. Solvatochromism effect of emission spectra for **2-PyBP** in solvents with varying polarity (A) and CIE 1931 chromaticity diagram (B).

Figure S21. Solvatochromism effect of emission spectra for **1-BuPyBP** in solvents with varying polarity (A) and CIE 1931 chromaticity diagram (B).

Figure S22. Solvatochromism effect of emission spectra for **2-BuPyBP** in solvents with varying polarity (A) and CIE 1931 chromaticity diagram (B).

Figure S23. The comparison of red-shift behaviors of four luminogens from cyclohexane to DMF based on substituent and position-dependent effects.

Figure S24. (A) Normalized fluorescence emission spectra of four luminogens and crystal of **1-PyBP**; (B) Effect of concentration on the fluorescence emission spectra of **2-PyBP** recorded in THF at room temperature; (C) Plots of maximum emission wavelength (black circle) and emission intensity (red circle) of **2-PyBP** in different concentrations; (D) Intermolecular interactions in crystals of **1-PyBP**.

Figure S25. (left) Effect of concentration on the fluorescence emission spectra of **1-PyBP** recorded in THF at room temperature; (right) plots of maximum emission wavelength and emission intensity in different concentrations.

Figure S26. (A) Effect of concentration on the fluorescence emission spectra of **1-BuPyBP** recorded in THF at room temperature; (B) plots of maximum emission wavelength and emission intensity in different concentrations.

Figure S27. (A) Effect of concentration on the fluorescence emission spectra of **2-BuPyBP** recorded in THF at room temperature; (B) plots of maximum emission wavelength and emission intensity in different concentrations.

Figure S28. Fluorescence decay profiles of **1-PyBP** (A), **2-PyBP** (B), **1-BuPyBP** (C) and **2-BuPyBP** (D).

Figure S29. The normalized PL and MCL spectra of **1-PyBP**.

Figure S30. The normalized PL and MCL spectra of **2-PyBP**.

Figure S31. The normalized PL and MCL spectra of **1-BuPyBP**.

Figure S32. PXRD patterns of as-prepared powder of **2-PyBP** and **2-BuPyBP** after grinding and fuming data.

Figure S33. PXRD pattern of as-prepared powder **1-BuPyBP** after grinding and fuming

data.

Figure S34. Reversible switching emission of pristine powder of **1-PyBP** (A) and **2-PyBP** (B) by repeating grinding–fuming cycles.

Figure S35. Frontier-molecular-orbital distributions and energy level diagrams for **1-PyBP**, **2-PyBP**, **1-BuPyBP**, and **2-BuPyBP** by DFT calculations.

Experimental

All melting points (Yanagimoto MP-S1) are uncorrected. ^{1}H NMR spectra (400 MHz) were recorded on a Nippon Denshi JEOL FT-300 NMR spectrometer with $SiMe_4$ as an internal reference: *J*-values are given in Hz. UV-vis spectra were recorded on a Perkin Elmer Lambda 19 UV/VIS/NIR spectrometer. Mass spectra were obtained on a Nippon Denshi JMS-01SA-2 spectrometer at 75 eV using a direct-inlet system. Gas–liquid chromatograph (GLC) analyses were performed by Shimadzu gas chromatograph, GC-14A; silicone OV^{-1}, 2 m; programmed temperature rise, 12°C min^{-1}; carrier gas nitrogen, 25 mL min^{-1}. Elemental analyses were performed by Yanaco MT-5.

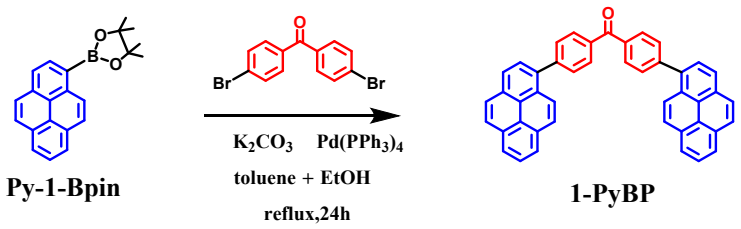

Scheme S1. The synthetic route of 1-PyBP

***Synthesis of compound* 1-PyBp** 4,4,5,5-Tetramethyl-2-(pyren-1-yl)-1,3,2-dioxaborolane (328 mg, 1.0 mmol.), bis(4-bromophenyl)methanone (136 mg, 0.4 mmol.) and $Pd(PPh_3)_4$ (46.2 mg, 0.04 mmol.) were added to toluene (20 mL) and EtOH (10 mL), in a 100-mL round-bottomed flask. Also add H_2O (20 mL) to potassium carbonate (5.7 g, 41 mmol) and mix the solutions together in the round bottom flask. Then the reaction mixture was heated under reflux for 24 h. The reaction solution was cooled to room temperature and added 100 ml ice water. The solution was extracted several times with DCM. The combined organic layers were dried over anhydrous $MgSO_4$. After filtration and evaporation of the solvent under reduced pressure, the product was purified by column chromatography using DCM/PE ether (1:2 v/v) as eluent. A pale yellow solid was obtained in 51.5% yield (146.5 mg); Mp 272–274 °C; ^{1}H NMR (400 MHz, $CDCl_3$, ppm) δ_H = 8.29 (d, *J* = 8.0 Hz, 2H), 8.23 (m, 6H), 8.16 (m, 8H), 8.10 (d, *J* = 9.2 Hz 2H), 8.06 (m,

4H), 7.84 (d, J = 8.4 Hz, 4H); ^{13}C NMR (100 MHz, $CDCl_3$, ppm): δ_C = 145.6, 136.4, 131.5, 131.2, 131.1, 131.0, 130.9, 130.8, 130.7, 130.3, 128.5, 128.4, 128.0, 127.9, 127.4, 127.3, 126.2, 125.4, 125.1, 125.0, 124.8, 124.7; FAB-MS: m/z calcd for $C_{45}H_{26}O$ 582.7020 [M^+]; found 582.1974 [M^+].

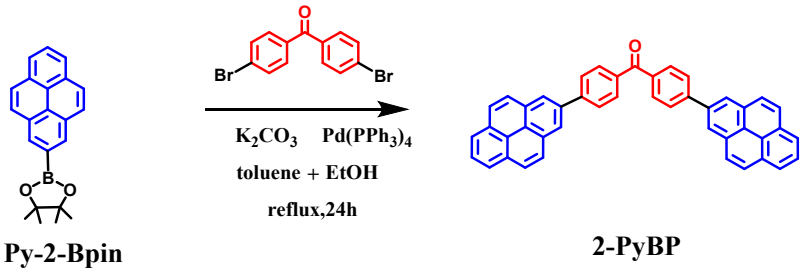

Py-2-Bpin　　2-PyBP

Scheme S2. The synthetic route of 2-PyBP

2-**PyBp** was obtained as a white solid by column chromatographed over silica gel from CH_2Cl_2/PE (1:2.5, v/v), (yield, 50.6%); Mp 326–328 °C; ^{1}H NMR (400 MHz, $CDCl_3$) δ = 8.49 (s, 4H), 8.23 (d, J = 7.6 Hz, 4H), 8.18 (d, J = 8.8 Hz, 4H), 8.15 (d, J = 8.8 Hz, 4H), 8.11 (d, J = 8.8 Hz, 4H), 8.09-8.06 (m, 4H), 8.04 (d, J = 8.0 Hz, 2H). ^{13}C NMR (100 MHz, DMSO, ppm): δ_C = 158.7, 143.8, 136.0, 135.5, 130.7, 130.1, 130.0, 129.5, 127.4, 127.2, 127.0, 126.0, 124.8, 122.9, 119.3; FAB-MS: m/z calcd for $C_{45}H_{26}O$ 582.7020 [M^+]; found 582.1974 [M^+].

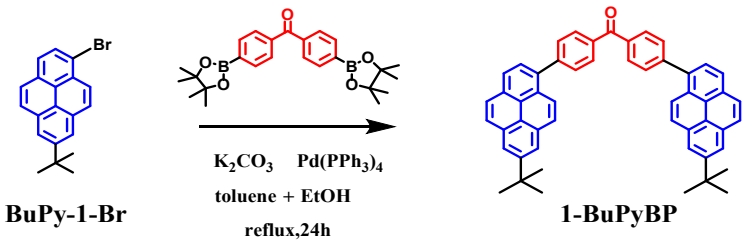

BuPy-1-Br　　1-BuPyBP

Scheme S3. The synthetic route of 1-BuPyBP

1-**BuPyBp** was obtained as a yellow solid by column chromatographed over silica gel from CH_2Cl_2/PE (1:2.5, v/v), (yield, 68.4%); Mp 174–176 °C; ^{1}H NMR (400 MHz, $CDCl_3$) δ 8.29−8.23 (m, 6H), 8.21 (d, J = 9.3 Hz, 2H), 8.16 (d, J = 8.2 Hz, 4H), 8.11 (s, 4H), 8.07 (d, J = 9.3 Hz, 2H), 8.01 (d, J = 7.8 Hz,

2H), 7.84 (d, J = 8.2 Hz, 4H), 1.60 (s, 18H). ^{13}C NMR (100 MHz, $CDCl_3$, ppm): δ_C = 136.4, 136.2, 131.3, 130.9, 130.8, 130.7, 130.3, 128.3, 128.2, 128.0, 127.3, 127.1, 124.9, 124.7, 123.1, 122.7, 122.4, 35.3, 32.0. FAB-MS: m/z calcd for $C_{53}H_{42}O$ 694.3236 [M^+]; found 694.3223 [M^+].

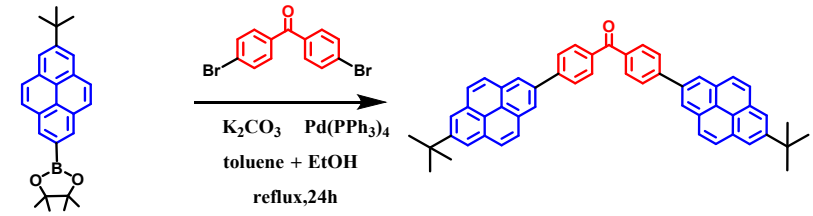

BuPy-2-Bpin **2-BuPyBP**

Scheme S4. The synthetic route of 2-BuPyBP

2-BuPyBp was obtained as a white solid by column chromatographed over silica gel from CH_2Cl_2/PE (1:2.5, v/v), (yield, 62.7%); Mp 254–276 °C; ^{1}H NMR (400 MHz, $CDCl_3$) δ_H = 8.47 (d, J = 15.2 Hz, 4H), 8.29−8.23 (m, 4H), 8.17 (t, J = 7.0 Hz, 8H), 8.15−8.12 (m, 4H), 8.10 (s, 4H), 8.08−8.02 (m, 4H), 1.57 (s, 18H); ^{13}C NMR (100 MHz, $CDCl_3$, ppm): δ_C = 131.7, 131.5, 131.2, 130.9, 130.1, 128.3, 128.1, 127.9, 127.5, 127.4, 126.2, 125.4, 123.7, 123.5, 122.7, 35.3, 32.0.FAB-MS: m/z calcd for $C_{53}H_{42}O$ 694.3236 [M^+]; found 694.3223 [M^+].

X-ray crystallography

A suitable single crystal of **1-PyBP** was obtained from a mixed dichloromethane/hexane solution. Single-crystal X-ray diffraction data were collected at 100(2) K on a XtaLAB Synergy-S, Dualflex, HyPix-6000HE diffractometer using Cu K radiation (λ = 1.5406 Å). The crystal was mounted on nylon CryoLoops with Paraton-N. The data collection and reduction were carried out using CrysAlisPro (Rigaku OD, 2019). A multi-scan absorption correction was applied to the collected reflections. Using Olex2, 52 the structure was solved using the ShelXT53 structure solution program using

Intrinsic Phasing and refined using the ShelXL54 refinement package using Least Squares minimisation. All non-hydrogen atoms were refined anisotropically. The organic hydrogen atoms were generated geometrically. See Table S1 (ESI†) for crystal data. CCDC 2328745 (**1-PyBP**) contains supplementary crystallographic data for this paper. Copies of the details of the data can be obtained, free of charge, on application to CCDC, 12 Union Road, Cambridge CB2 1EZ, UK [fax: 144-1223-336033 or e-mail: deposit@ccdc.cam.ac.uk].

Table S1. Crystal data and structure refinement of **1-PyBP**

Compound	**1-PyBP**
Empirical formula	$C_{45}H_{26}O$
Formula weight	582.66
Crystal system	Triclinic
Space group	P-1
a[Å]	8.7621(8)
b[Å]	10.6742(11)
c[Å]	16.7270(18)
α[°]	80.613(3)
β[°]	82.954(3)
γ[°]	70.163(3)
Volume[Å^3]	1448.1(3)
Z	2
μ	0.078 mm^{-1}
F(000)	608
Crystal size [mm^3]	0.18 × 0.21 × 0.15
Dcalcd [Mg/m^3]	1.336
Temperature [K]	273(2)
Measured reflns	27715
Unique reflns	5686
Observed reflns	3712
Parameters	415

R(int)	0.0856
$R[I> 2\sigma(I)]$[a]	0.0466
$wR2$[all data][b]	0.1295
GOF on F^2	1.070

[a]$R_1 = \sum||F_o|-|F_c||$ (based on reflections with $F_o^2>2\sigma F^2$) [b]$wR_2 = [\sum[w(F_o^2-F_c^2)^2]/\sum[w(F_o^2)^2]]^{1/2}$; w $=1/[\sigma^2(F_o^2) + (0.095P)^2]$; $P = [\max(F_o^2, 0) + 2F_c^2]/3$(also with $F_o^2>2\sigma F^2$)

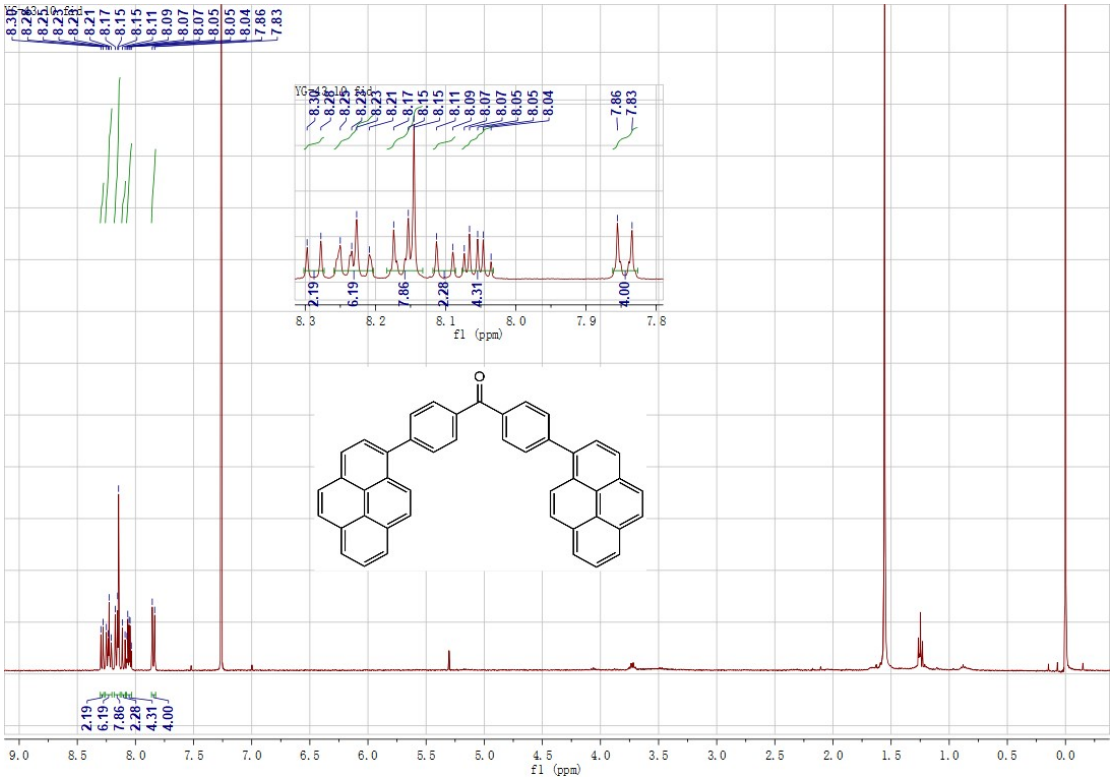

Figure S1. ^{1}H NMR spectrum of **1-PyBP** (400 MHz, 293 K, $CDCl_3$).

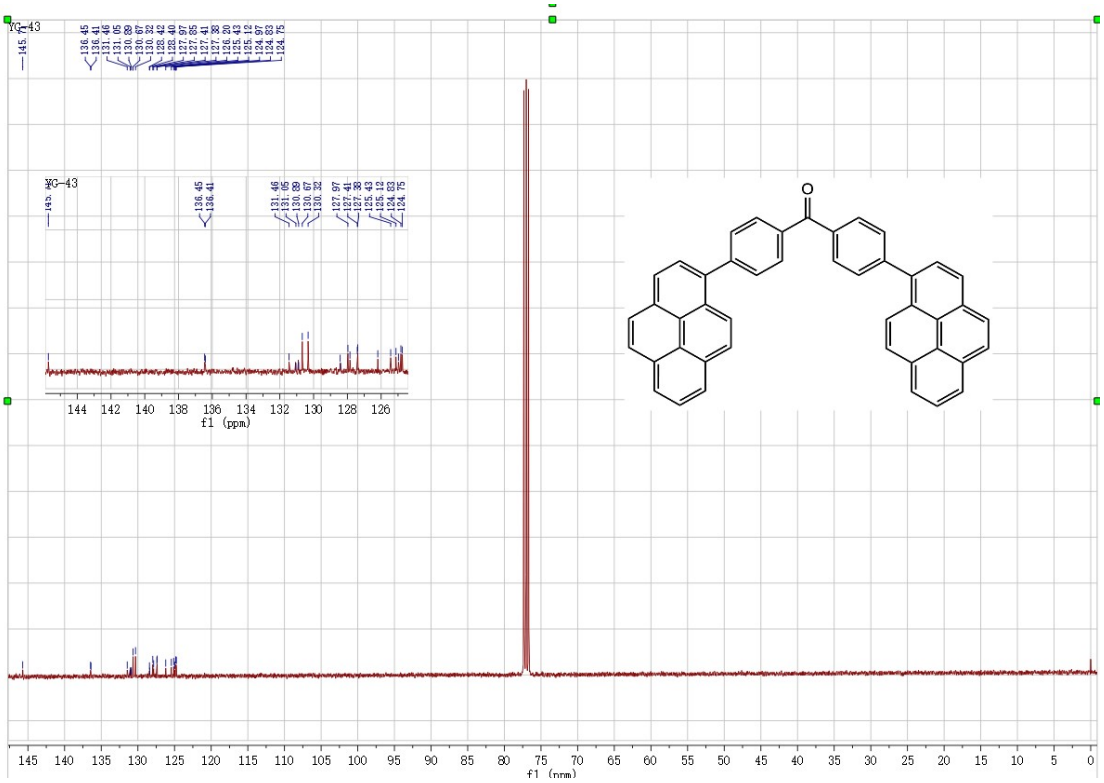

Figure S2. ^{13}C NMR spectrum of **1-PyBP** (100 MHz, 293 K, $CDCl_3$).

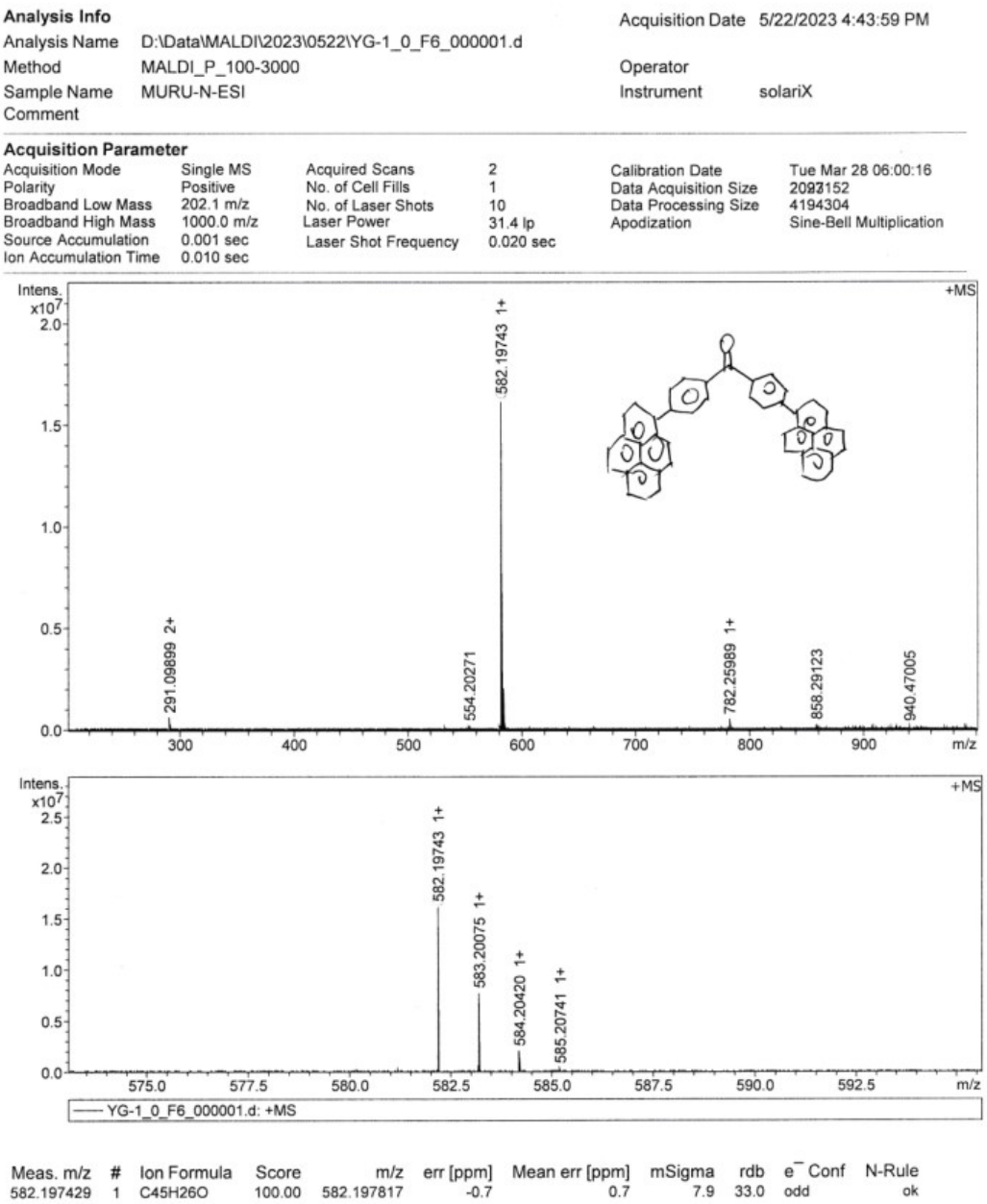

Figure S3. The high resolution MALDI-TOF-MS spectra of **1-PyBP**.

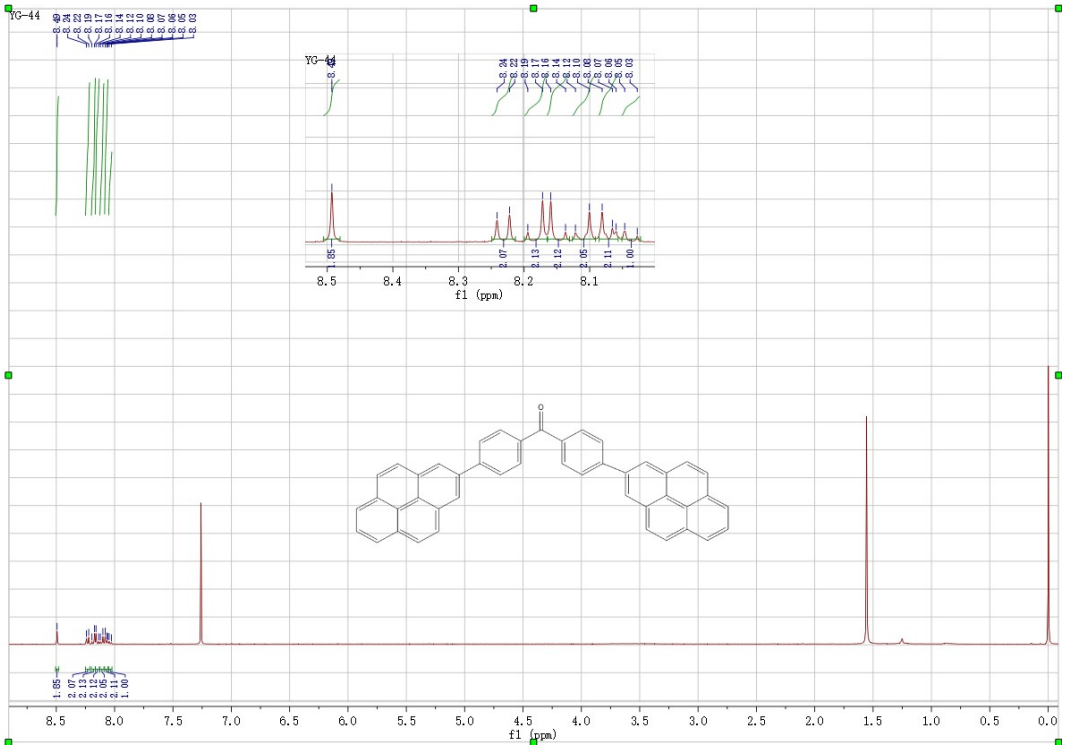

Figure S4. ^{1}H NMR spectrum of **2-PyBP** (400 MHz, 293 K, $CDCl_3$).

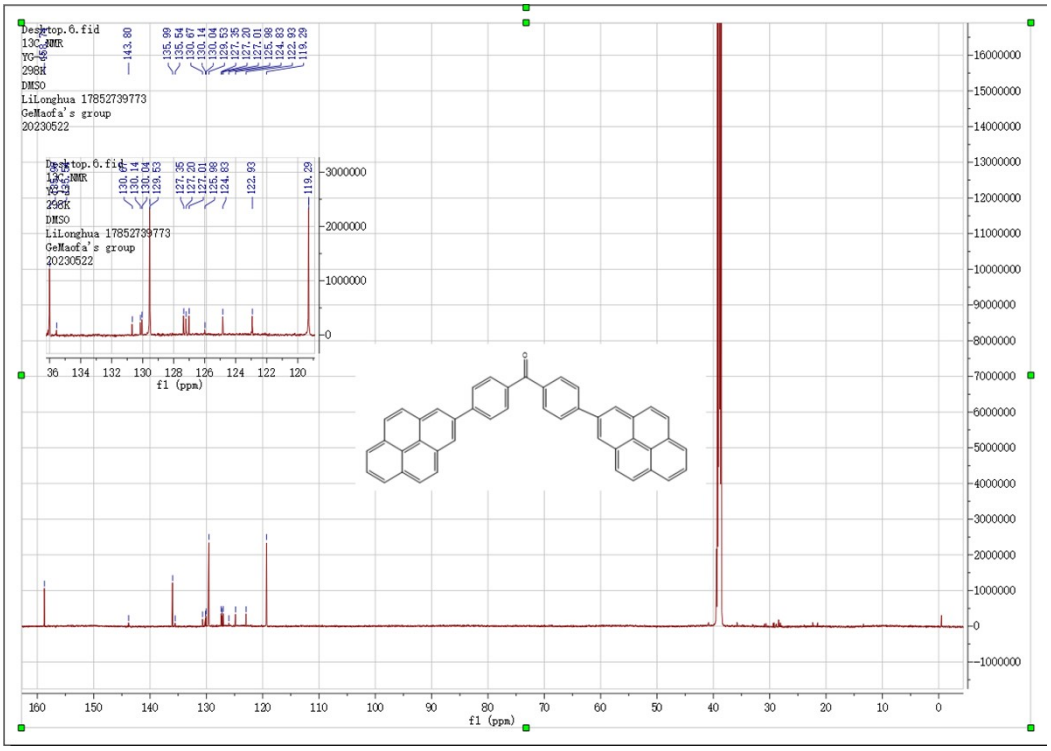

Figure S5. ^{13}C NMR spectrum of **2-PyBP** (100 MHz, 293 K, $CDCl_3$).

Analysis Info

Analysis Name	D:\Data\MALDI\2023\0522\YG-2_0_F7_000001.d	Acquisition Date	5/22/2023 4:44:43 PM
Method	MALDI_P_100-3000	Operator	
Sample Name	MURU-N-ESI	Instrument	solariX
Comment			

Acquisition Parameter

Acquisition Mode	Single MS	Acquired Scans	3	Calibration Date	Tue Mar 28 06:00:16
Polarity	Positive	No. of Cell Fills	1	Data Acquisition Size	2097152
Broadband Low Mass	202.1 m/z	No. of Laser Shots	10	Data Processing Size	4194304
Broadband High Mass	1000.0 m/z	Laser Power	31.4 lp	Apodization	Sine-Bell Multiplication
Source Accumulation	0.001 sec	Laser Shot Frequency	0.020 sec		
Ion Accumulation Time	0.010 sec				

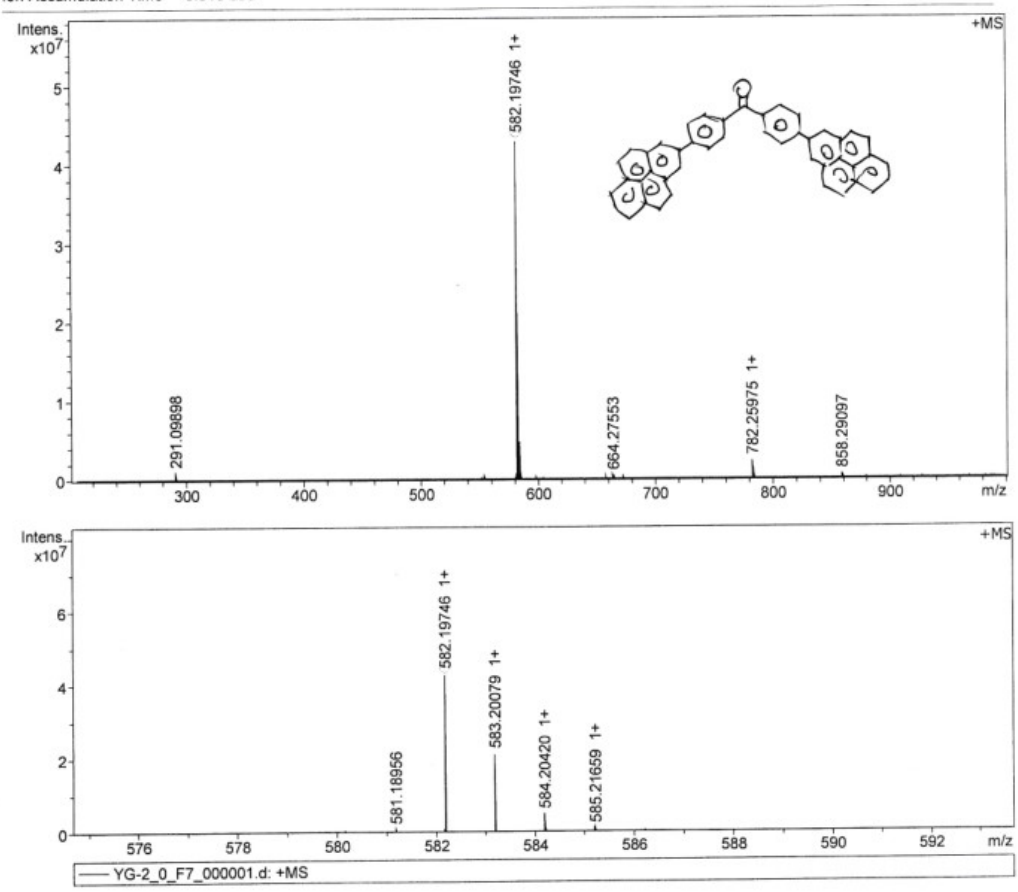

Meas. m/z	#	Ion Formula	Score	m/z	err [ppm]	Mean err [ppm]	mSigma	rdb	e⁻ Conf	N-Rule
582.197456	1	C45H26O	100.00	582.197817	-0.6	0.6	4.6	33.0	odd	ok

Figure S6. The high resolution MALDI-TOF-MS spectra of **2-PyBP**.

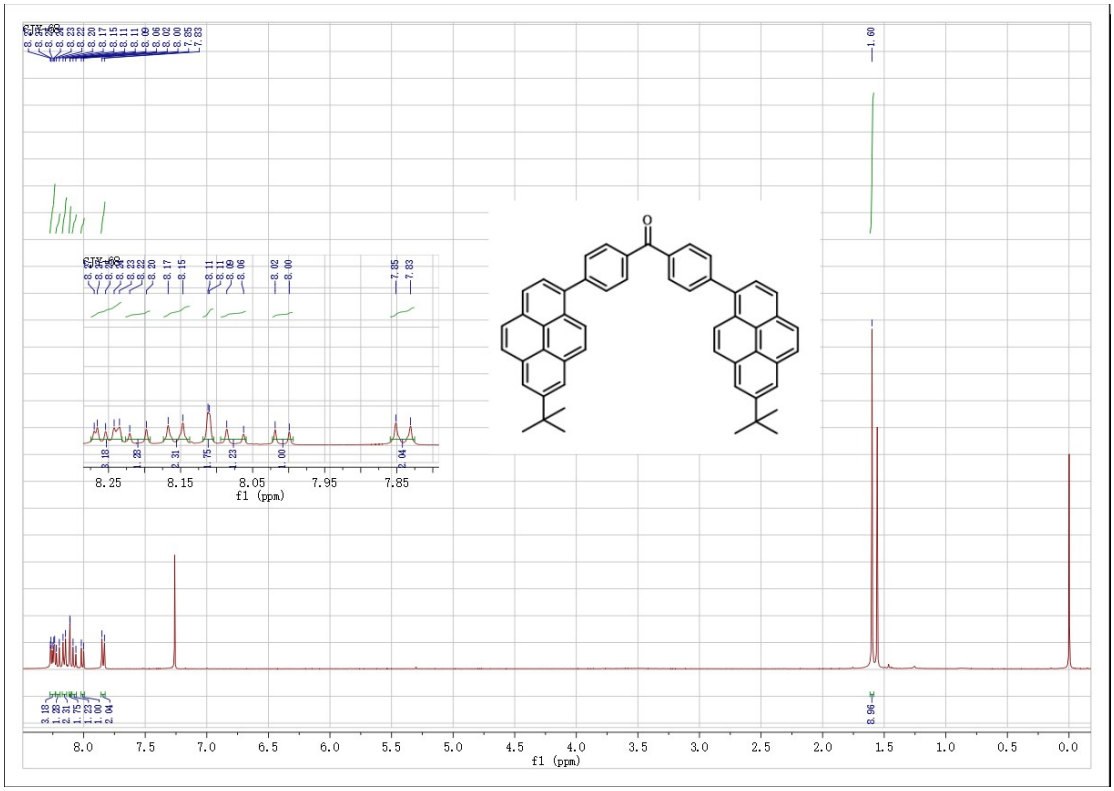

Figure S7. ^{1}H NMR spectrum of **1-BuPyBP** (400 MHz, 293 K, $CDCl_3$).

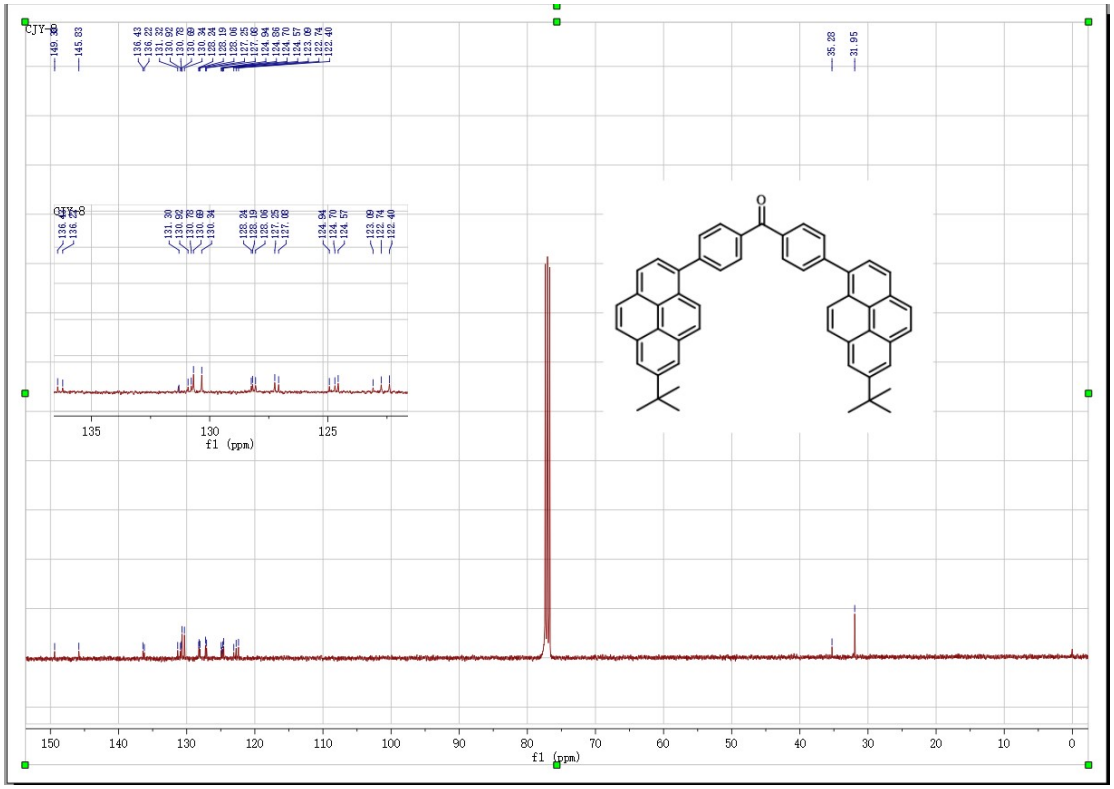

Figure S8. ^{13}C NMR spectrum of **1-BuPyBP** (100 MHz, 293 K, $CDCl_3$).

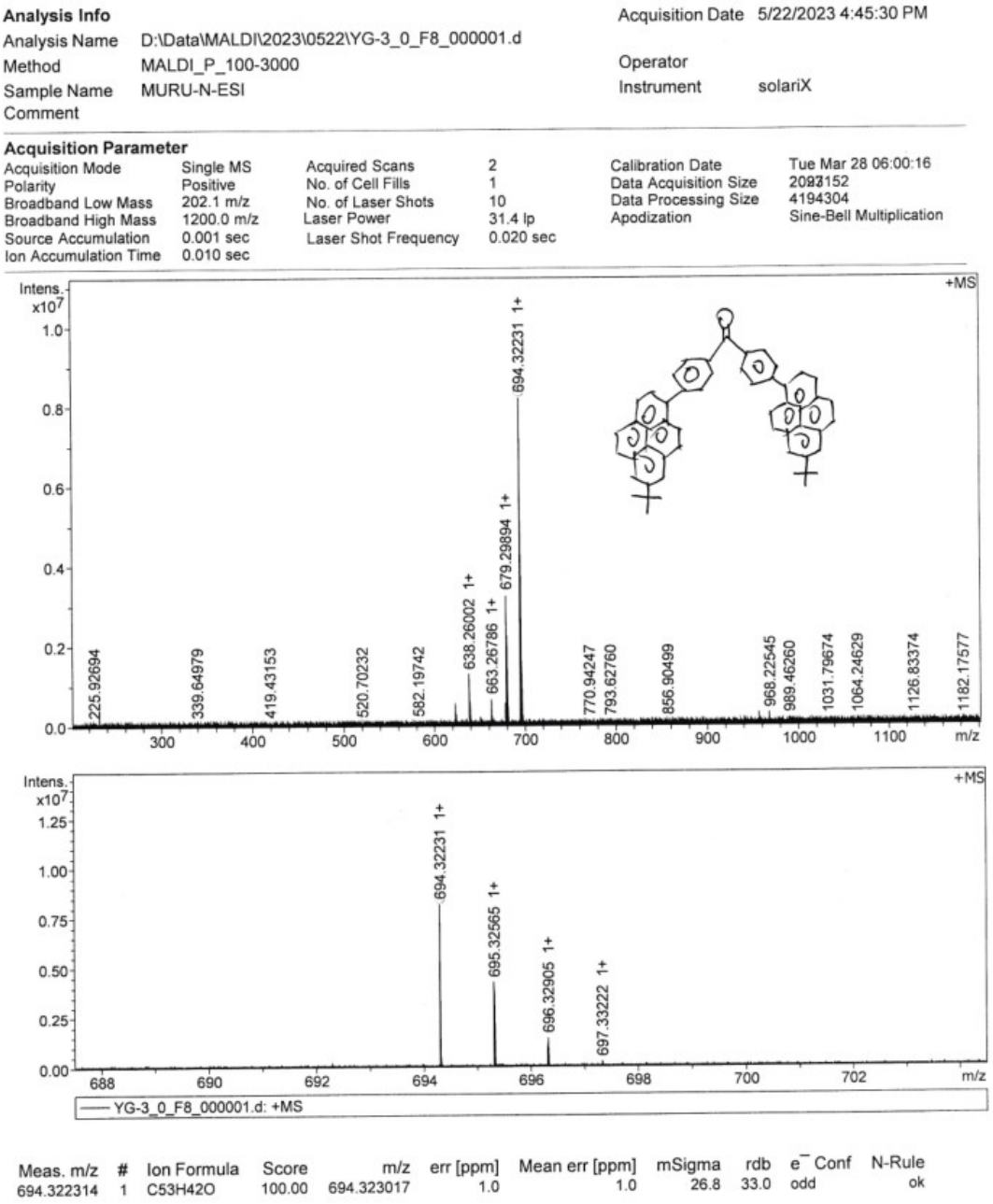

Figure S9. The high resolution MALDI-TOF-MS spectra of **1-BuPyBP**.

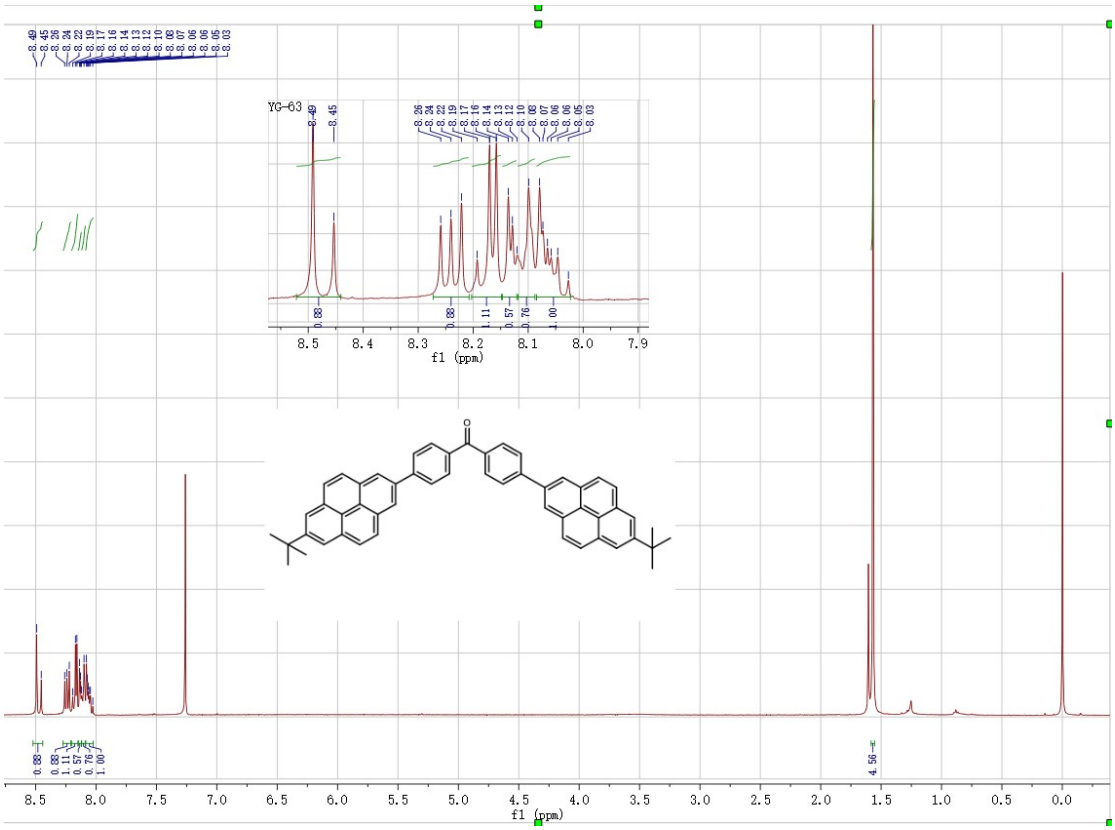

Figure S10. ^{1}H NMR spectrum of **2-BuPyBP** (400 MHz, 293 K, $CDCl_3$).

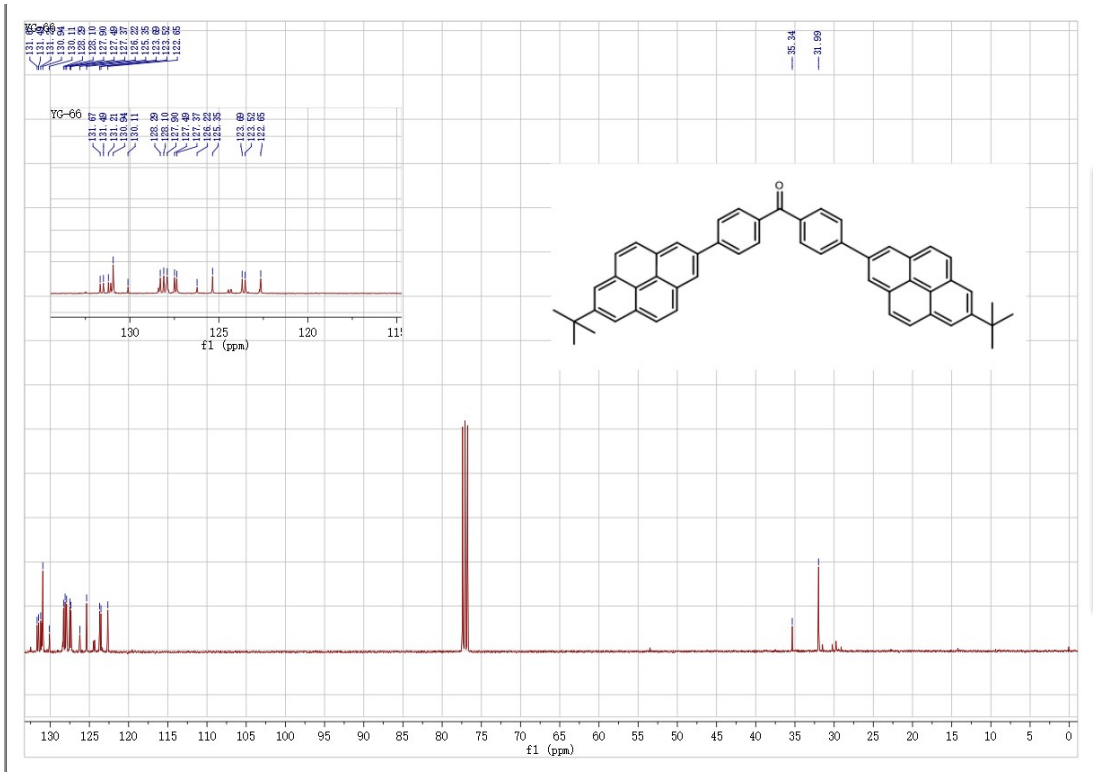

Figure S11. ^{13}C NMR spectrum of **2-BuPyBP** (100 MHz, 293 K, $CDCl_3$).

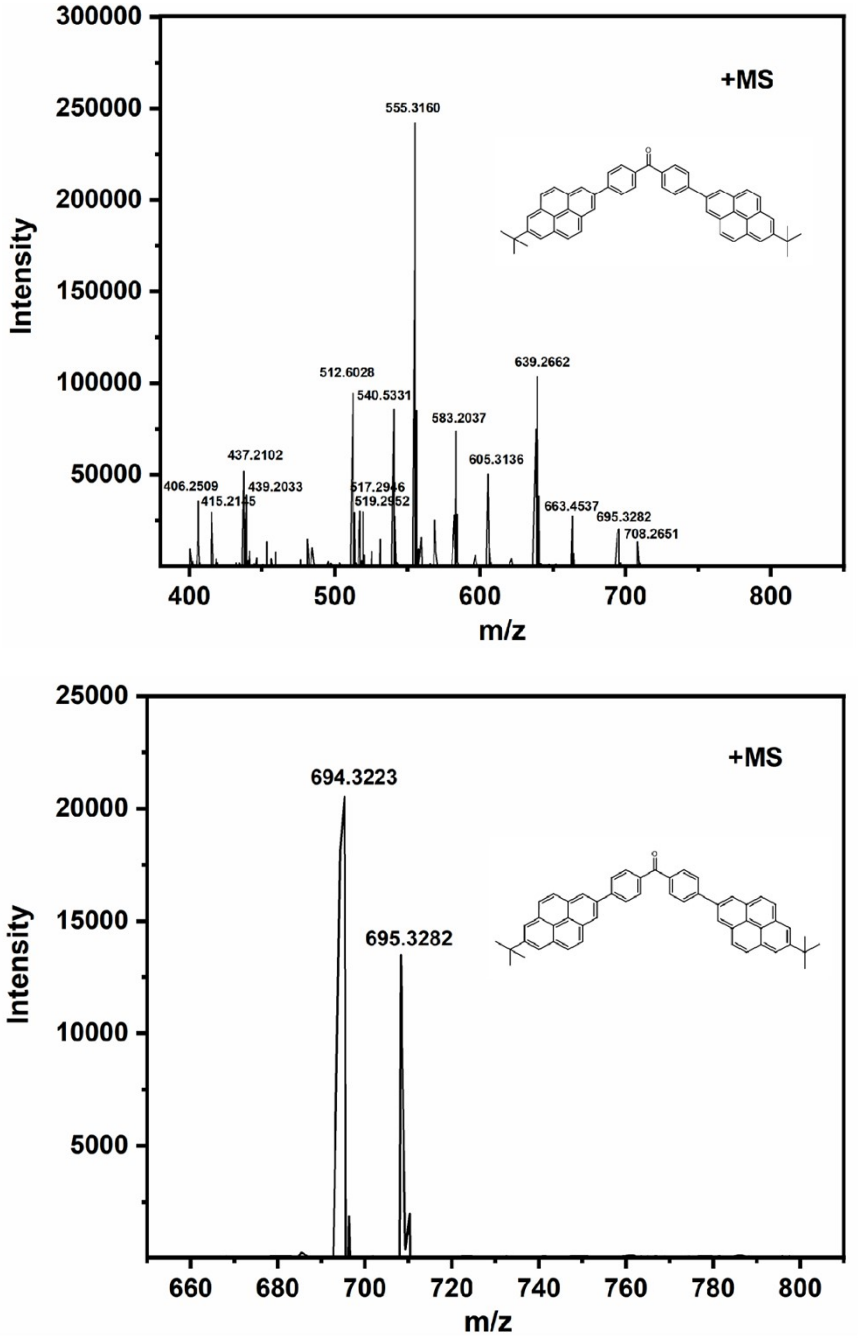

Figure S12. The high resolution MALDI-TOF-MS spectra of **2-BuPyBP**.

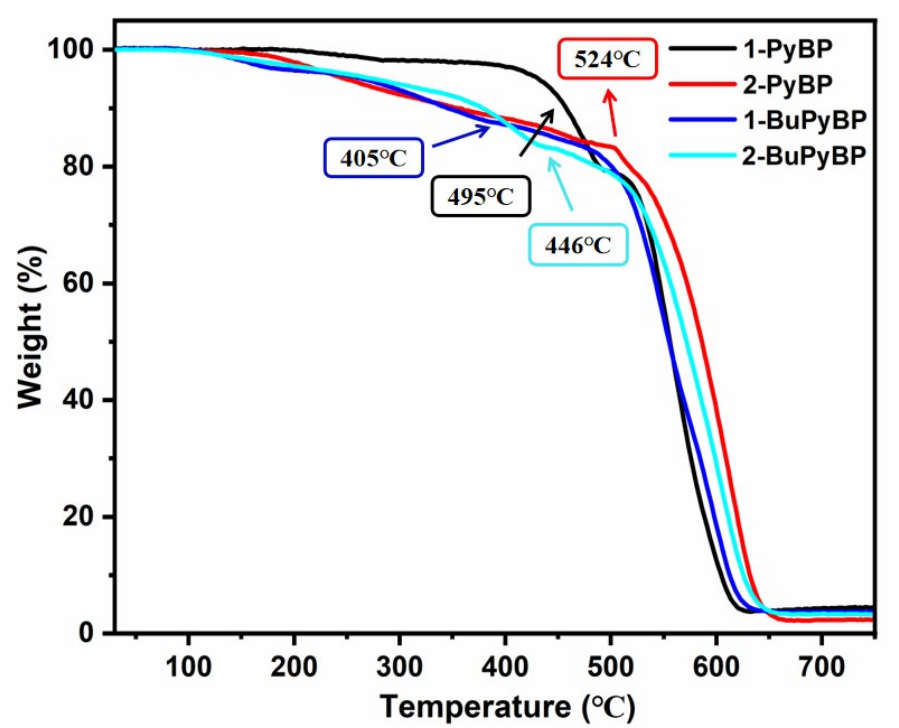

Figure S13. TGA analysis of **1–PyBP**, **2–PyBP**, **1-BuPyBP**, **2-BuPyBP**.

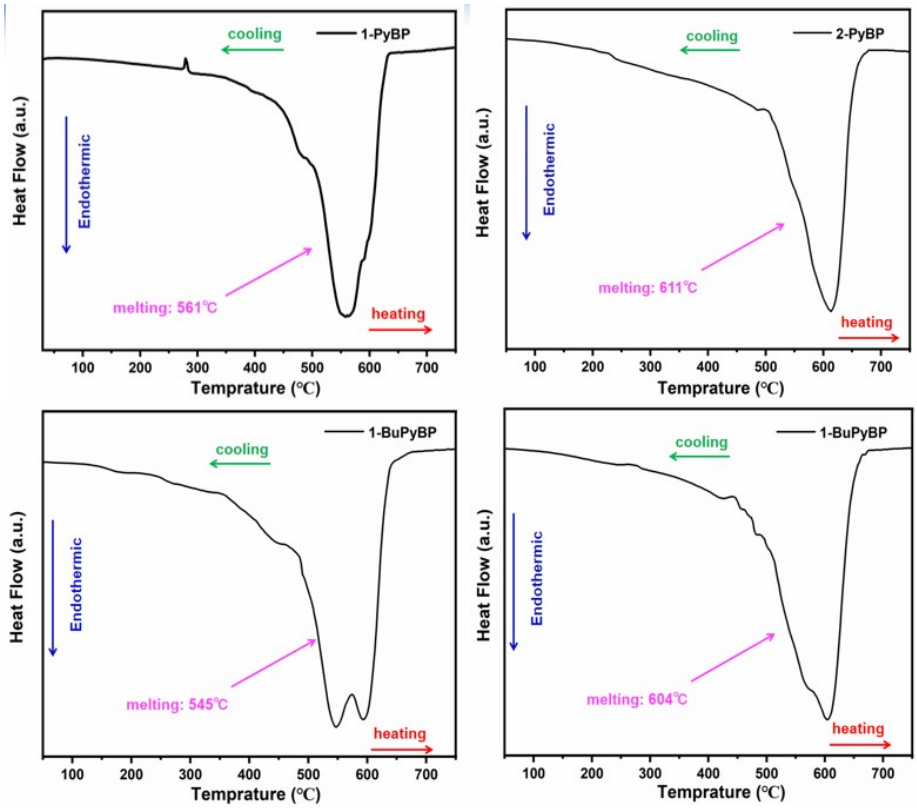

Figure S14. DSC analysis of **1–PyBP**, **2–PyBP**, **1-BuPyBP**, **2-BuPyBP**.

Table S2. The photophysical properties of **1–PyBP**, **2–PyBP**, **1-BuPyBP**, **2-BuPyBP**.

Comps	**λ_{abs} (nm)[a]**	**λ_{em} (nm)[b]**		**Stokes shift (nm)**		**Φ_{FL}(%)[c]**		**τ(ns)**	**K_r ($\times10^7S^{-1}$)**	**K_{nr} ($\times10^7S^{-1}$)**	**DFT (eV)[e]**		
	Solution	Solution	Pristine	Ground[d]	Solution	Solution	Pristine	Ground[d]	Solution /Solid	Solution /Solid	Solution /Solid	HOMO	LUMO	ΔE_g
1-PyBP	278,349	480	511 (537[f])	518	131	17.1	5.0 (1.7[f])	26.3	1.0628 /1.6537 (3.9120[f])	0.161/0.030, (0.004[f])	1.109/0.616, (0.256)	-5.36	-1.98	3.38
2-PyBP	323,339	458	469	499	119	0.5	0.3	31.7	1.6996 /1.8457	0.003/0.002	0.589/0.542	-5.47	-1.90	3.57
1-BuPyBP	290, 359	412,451	500	498	92	2.6	77.5	79.6	0.9882 /5.0570	0.026/0.153	0.962/0.204	-5.29	-1.94	3.35
2-BuPyBP	322, 338	416	454	483	78	3.6	0.5	49.2	3.8821/7.2605	0.009/0.001	0.258/0.137	-5.40	-1.83	3.57

[a] ~$\times10^{-5}$ M in THF, λ_{abs} is the absorption band appearing at the longest wavelength.

[b] ~$\times10^{-7}$ M in THF, λ_{em} is the fluorescence band appearing at the shortest wavelength.

[c] Absolute quantum yield (±1−3).

[d] Obtained by mechanical lapping.

[e] DFT/B3LYP/6-31G* using Gaussian.

[f] Crystalline state.

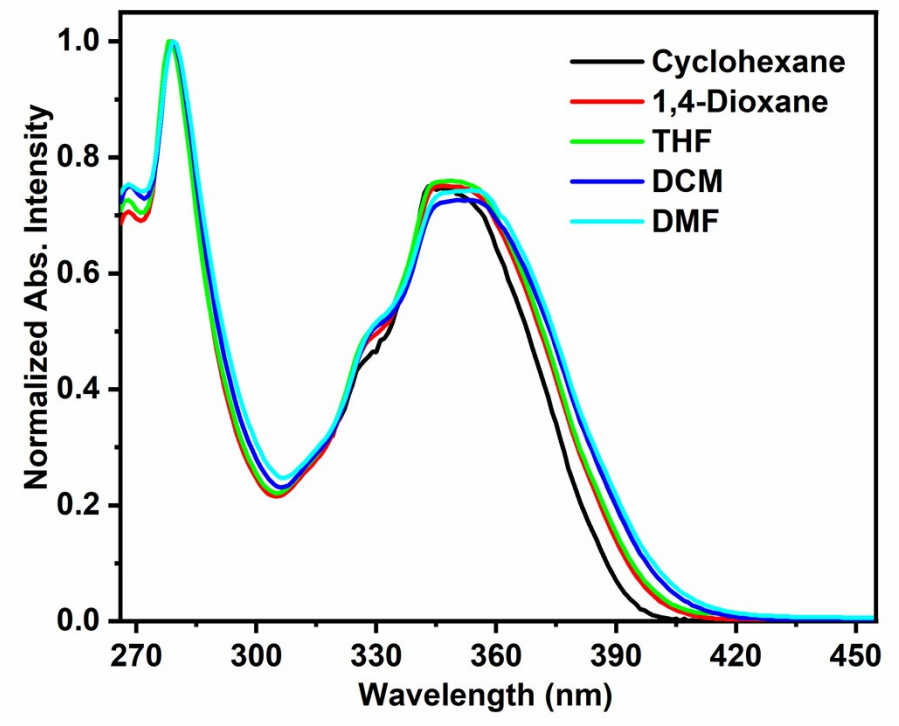

Figure S15. Solvatochromism effect of absorption spectra for **1-PyBP** in Cyclohexane, 1, 4-Dioxane, THF, DCM and DMF, respectively.

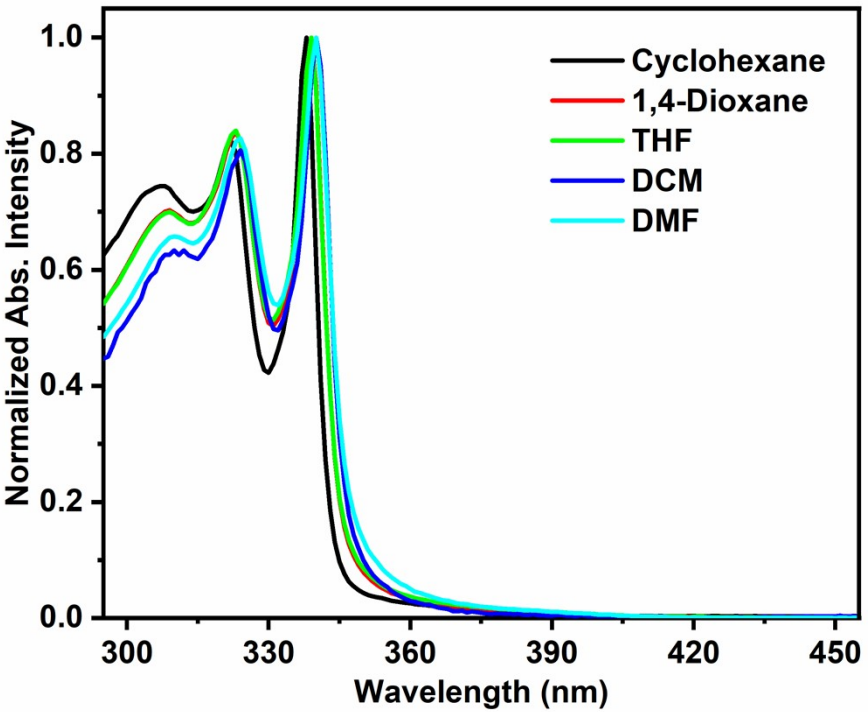

Figure S16. Solvatochromism effect of absorption spectra for **2-PyBP** in Cyclohexane, 1, 4-Dioxane, THF, DCM and DMF, respectively.

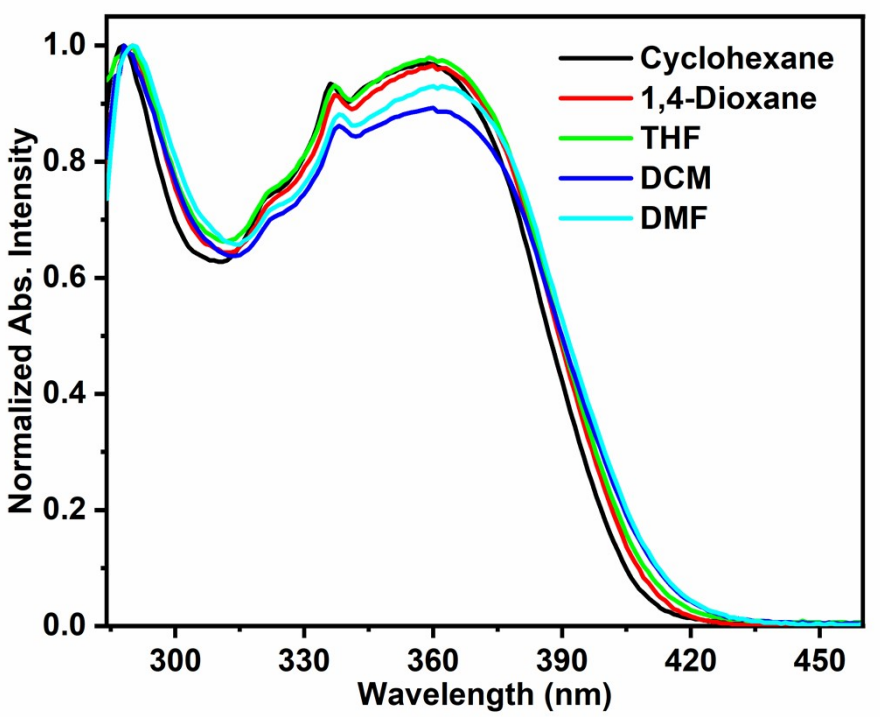

Figure S17. Solvatochromism effect of absorption spectra for **1-BuPyBP** in Cyclohexane, 1, 4-Dioxane, THF, DCM and DMF, respectively.

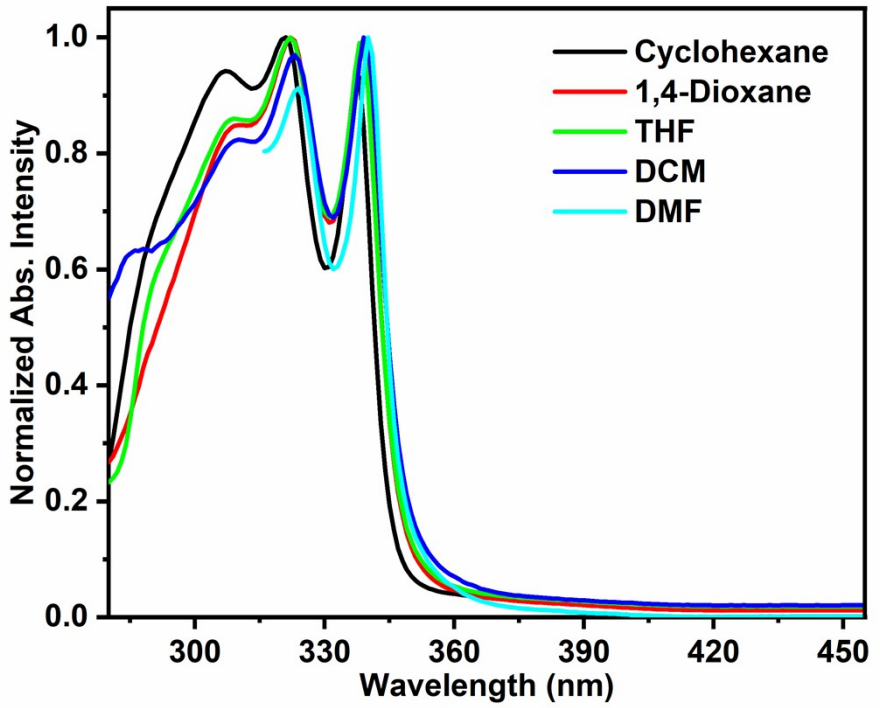

Figure S18. Solvatochromism effect of absorption spectra for **2-BuPyBP** in Cyclohexane, 1, 4-Dioxane, THF, DCM and DMF, respectively.

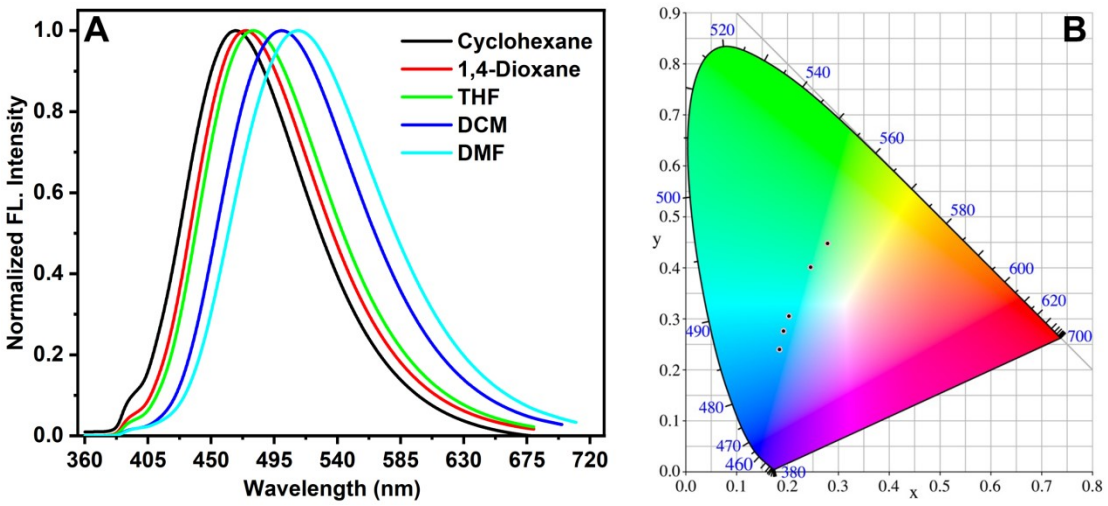

Figure S19. Solvatochromism effect of emission spectra for **1-PyBP** in solvents with varying polarity (A) and CIE 1931 chromaticity diagram (B).

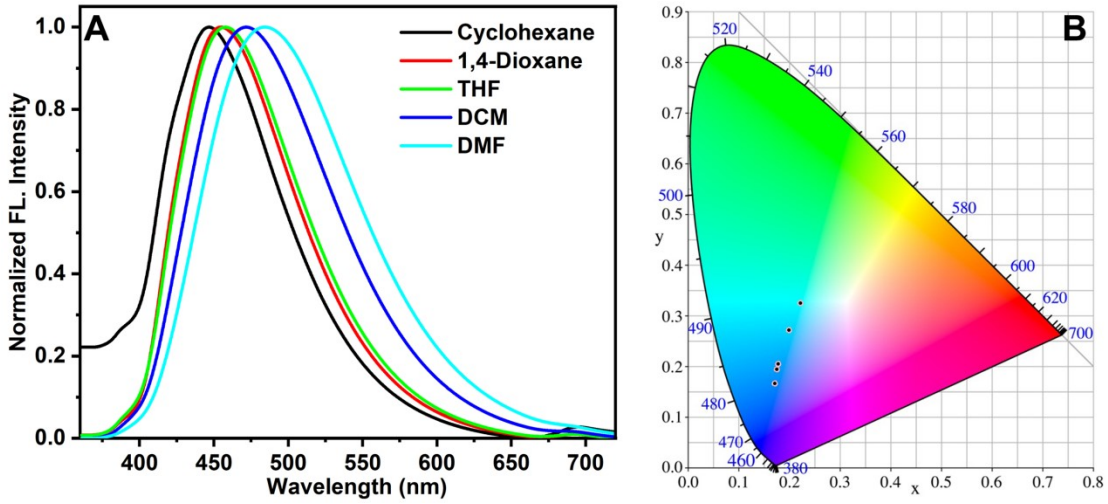

Figure S20. Solvatochromism effect of emission spectra for **2-PyBP** in solvents with varying polarity (A) and CIE 1931 chromaticity diagram (B).

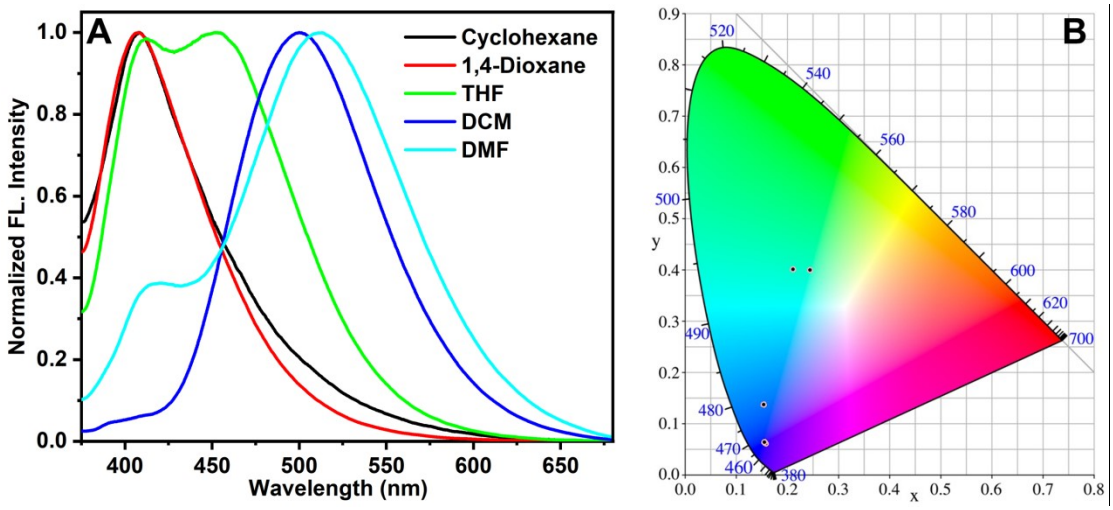

Figure S21. Solvatochromism effect of emission spectra for **1-BuPyBP** in solvents with varying polarity (A) and CIE 1931 chromaticity diagram (B).

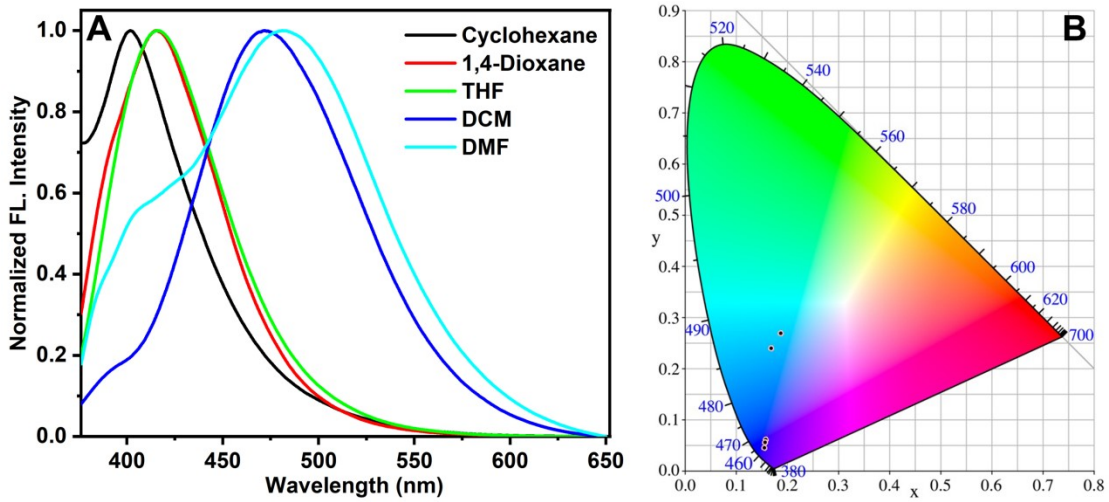

Figure S22. Solvatochromism effect of emission spectra for **2-BuPyBP** in solvents with varying polarity (A) and CIE 1931 chromaticity diagram (B).

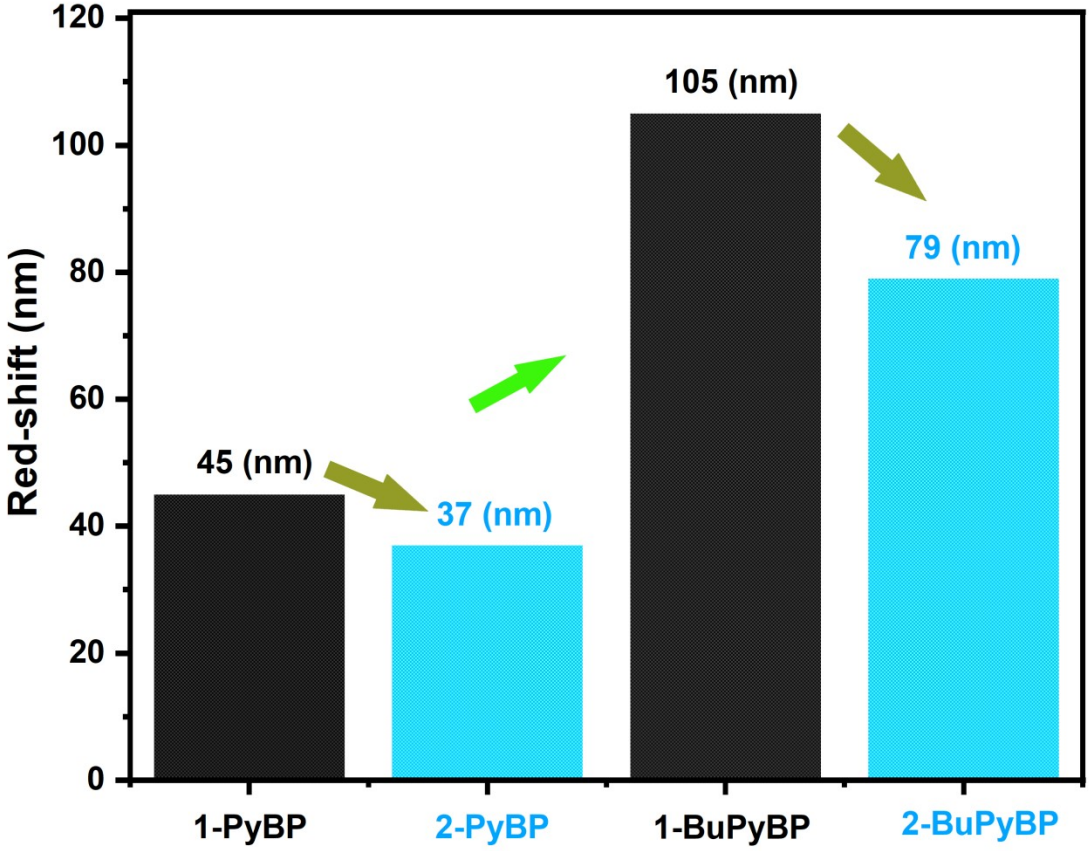

Figure S23. The comparison of red-shift behaviors of four luminogens from cyclohexane to DMF based on substituent and position-dependent effects.

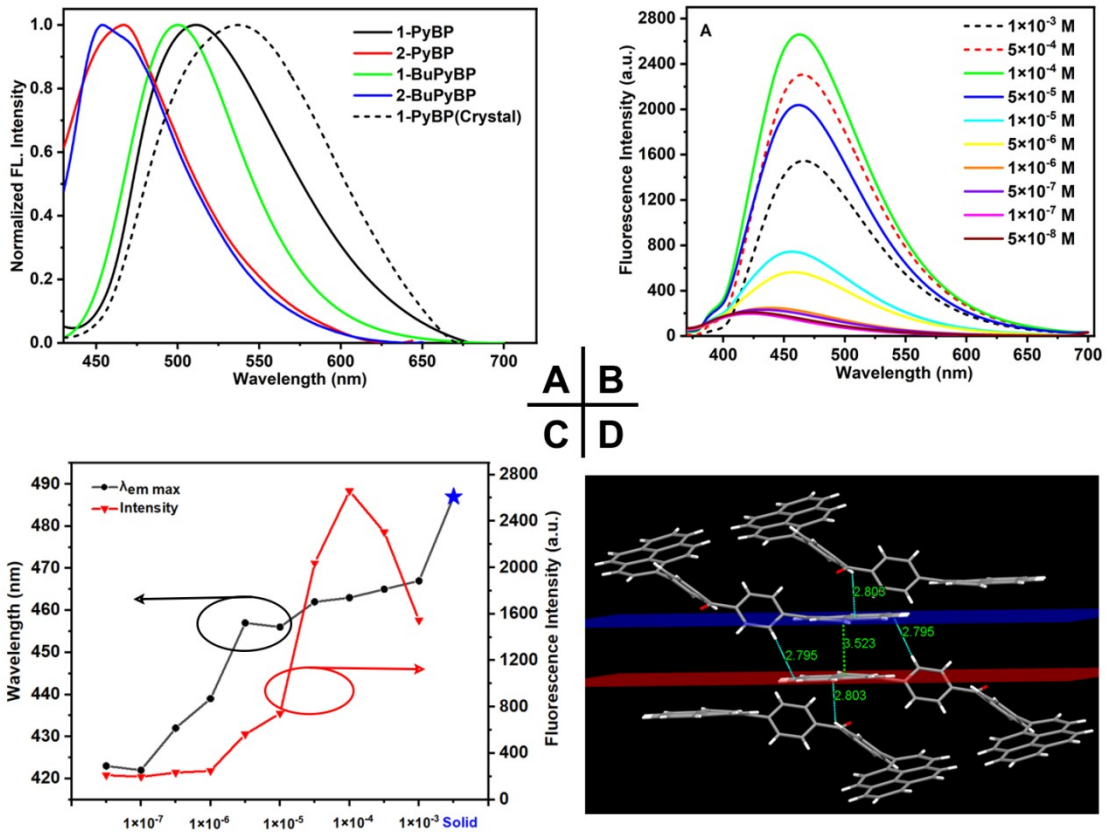

Figure S24. (A) Normalized fluorescence emission spectra of four luminogens and crystal of **1-PyBP**; (B) Effect of concentration on the fluorescence emission spectra of **2-PyBP** recorded in THF at room temperature; (C) Plots of maximum emission wavelength (black circle) and emission intensity (red circle) of **2-PyBP** in different concentrations; (D) Intermolecular interactions in crystals of **1-PyBP**.

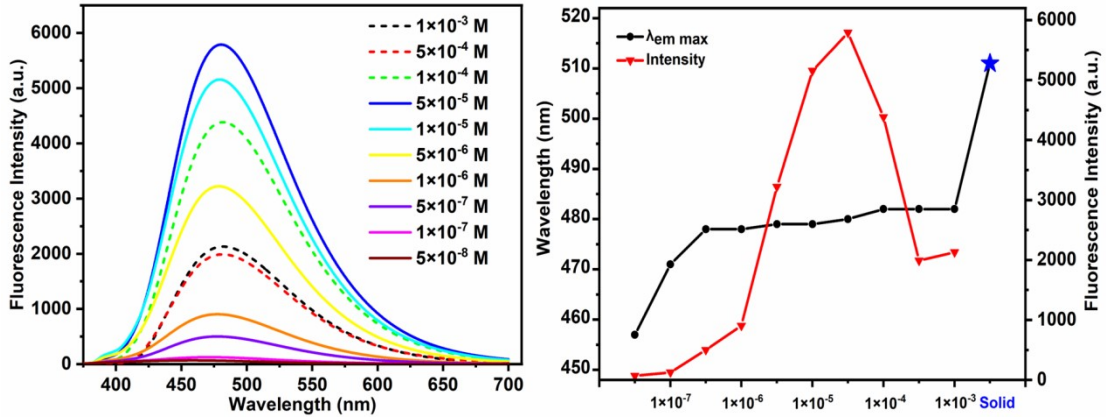

Figure S25. (left) Effect of concentration on the fluorescence emission spectra of **1-PyBP** recorded in THF at room temperature; (right) plots of maximum emission wavelength and emission intensity in different concentrations.

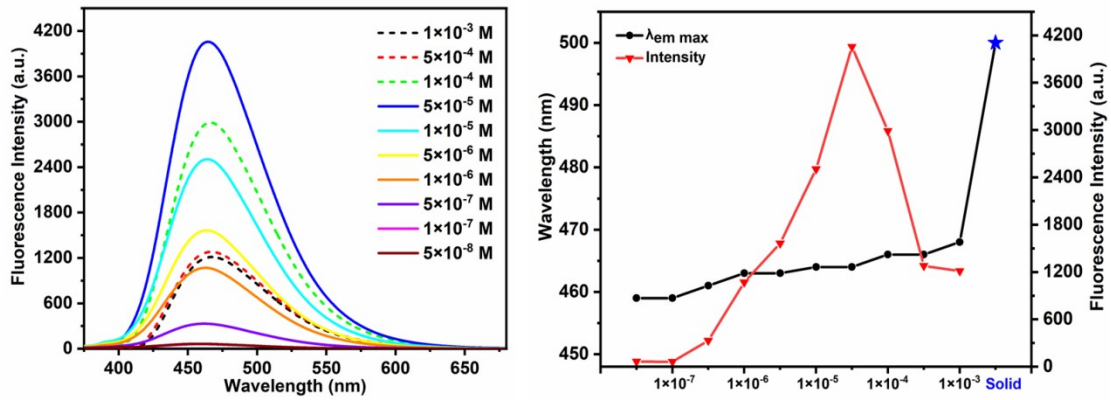

Figure S26. (A) Effect of concentration on the fluorescence emission spectra of **1-BuPyBP** recorded in THF at room temperature; (B) plots of maximum emission wavelength and emission intensity in different concentrations.

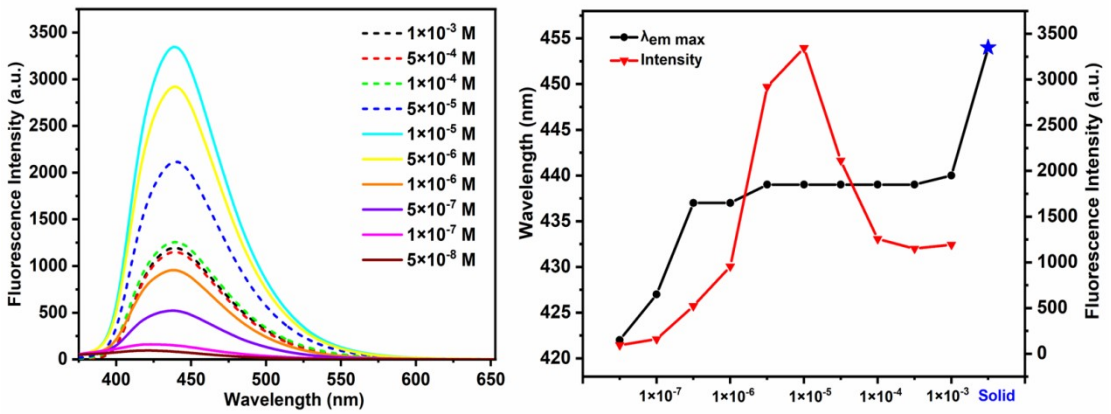

Figure S27. (A) Effect of concentration on the fluorescence emission spectra of **2-BuPyBP** recorded in THF at room temperature; (B) plots of maximum emission wavelength and emission intensity in different concentrations.

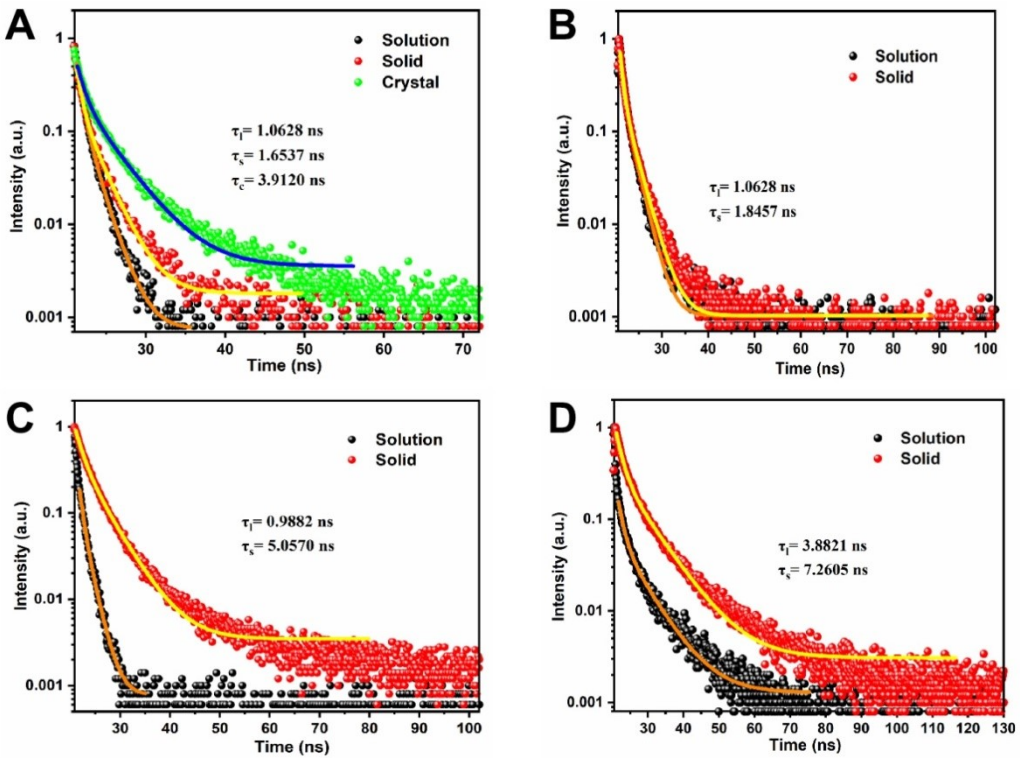

Figure S28. Fluorescence decay profiles of **1-PyBP** (A), **2-PyBP** (B), **1-BuPyBP** (C) and **2-BuPyBP** (D).

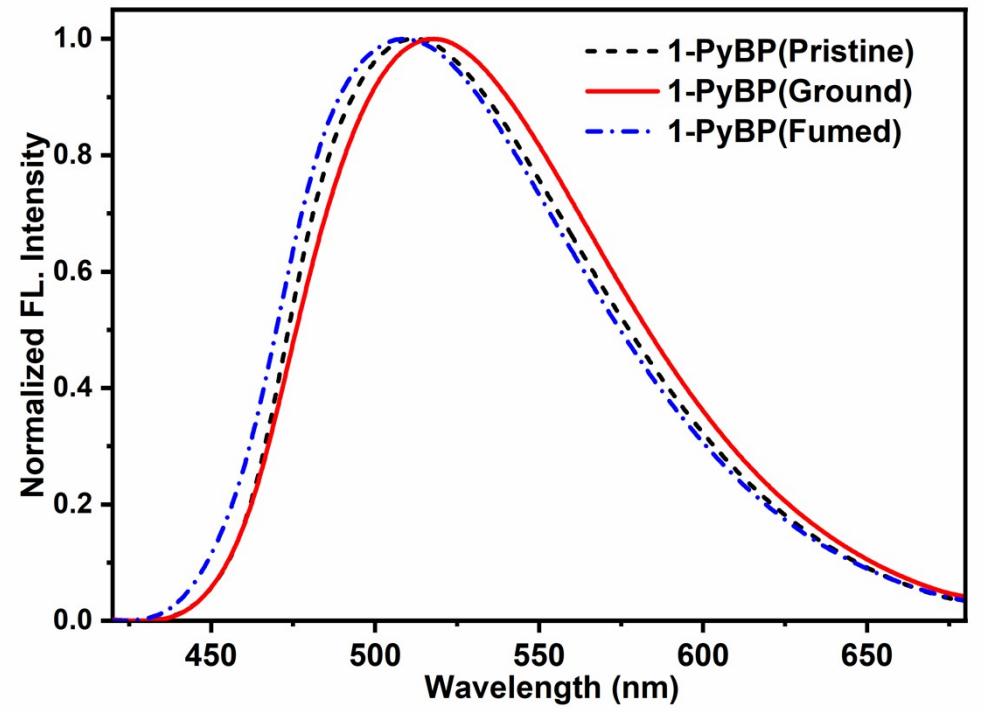

Figure S29. The normalized PL and MCL spectra of **1-PyBP**.

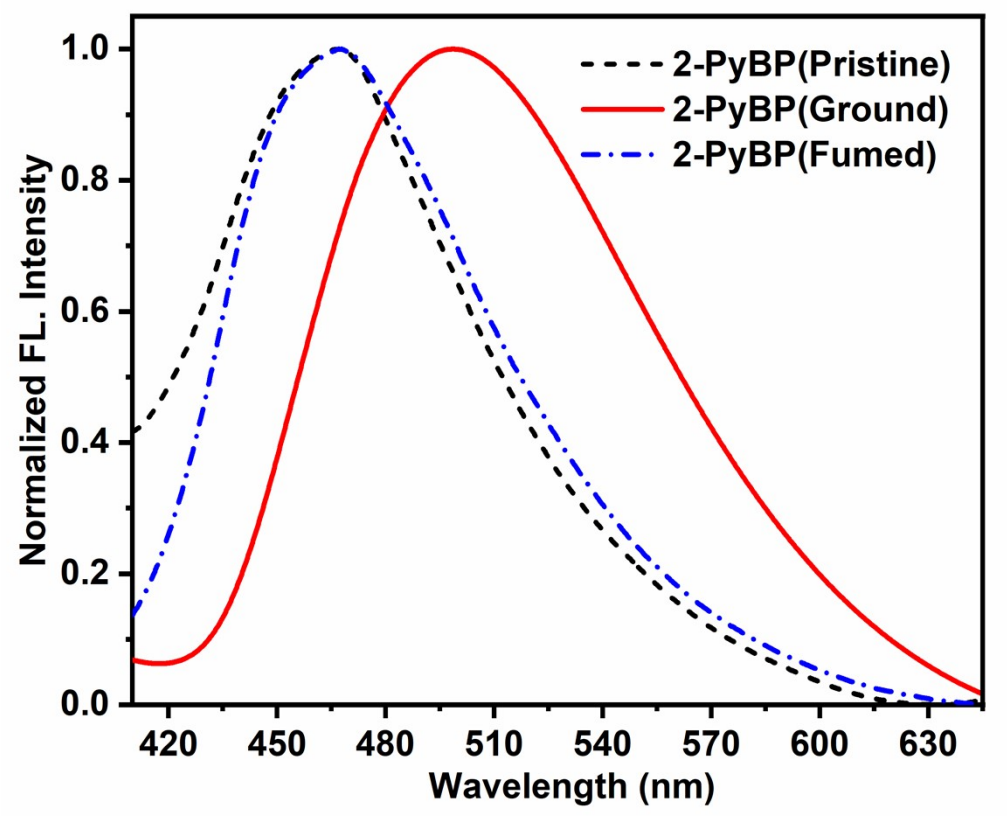

Figure S30. The normalized PL and MCL spectra of **2-PyBP**.

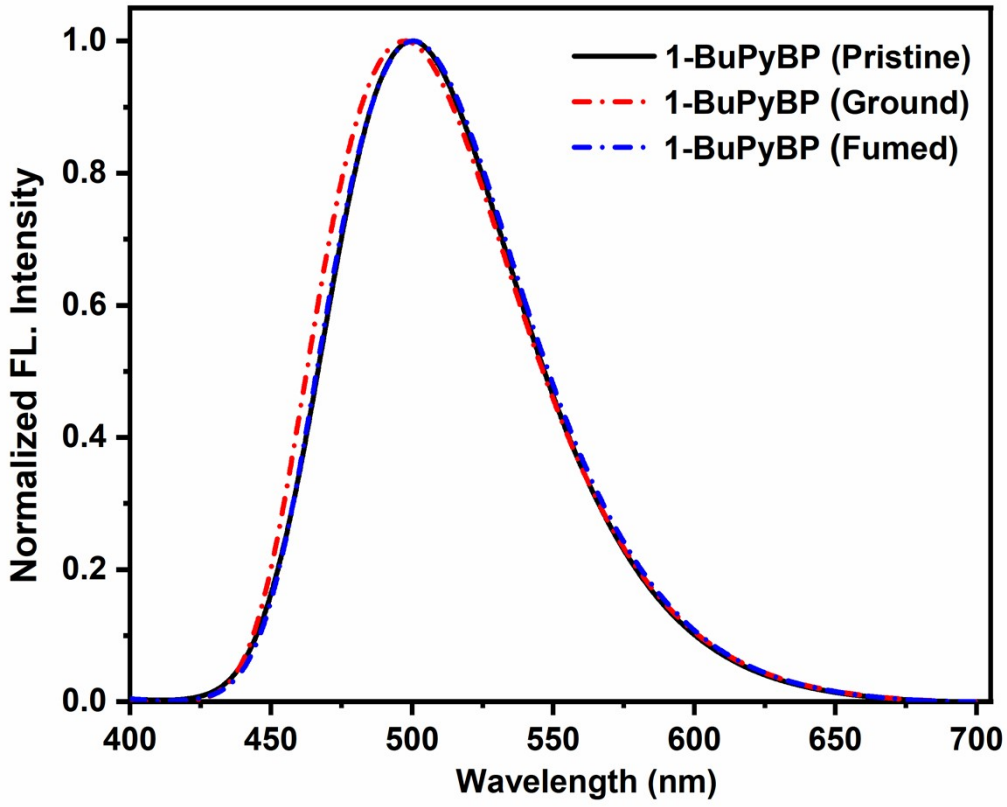

Figure S31. The normalized PL and MCL spectra of **1-BuPyBP**.

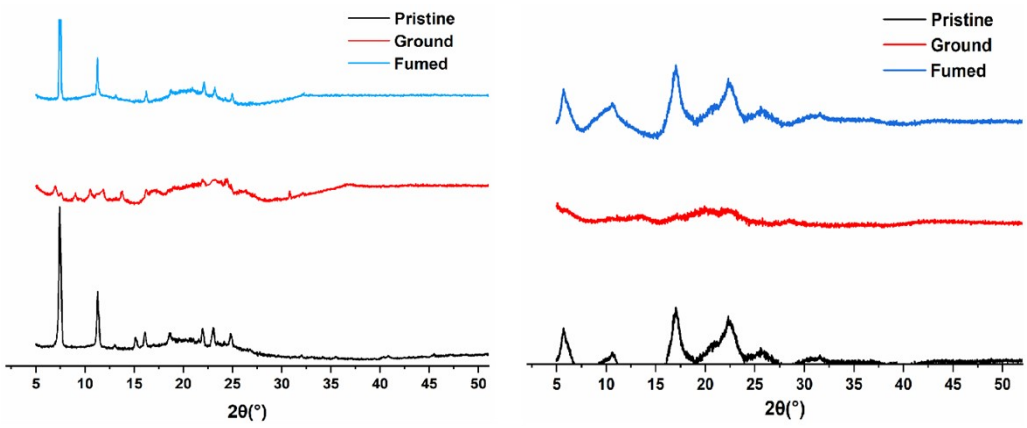

Figure S32. PXRD patterns of as-prepared powder of **2-PyBP** and **2-BuPyBP** after grinding and fuming data.

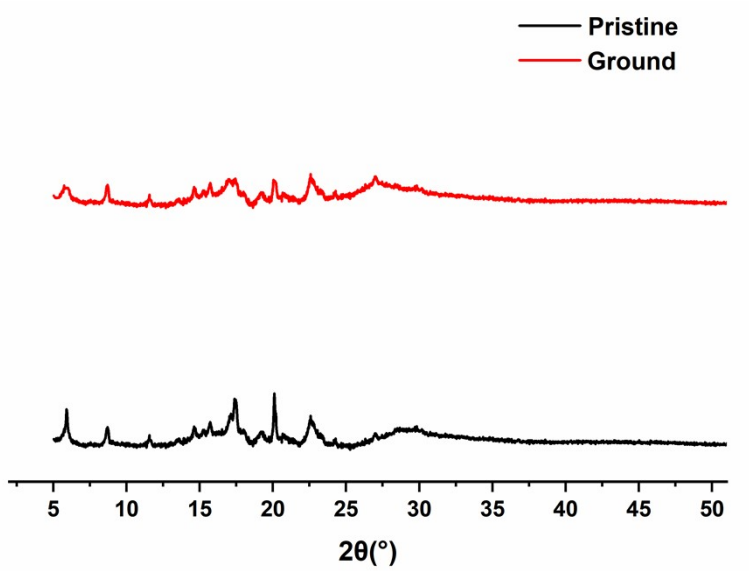

Figure S33. PXRD pattern of as-prepared powder **1-BuPyBP** after grinding and fuming data.

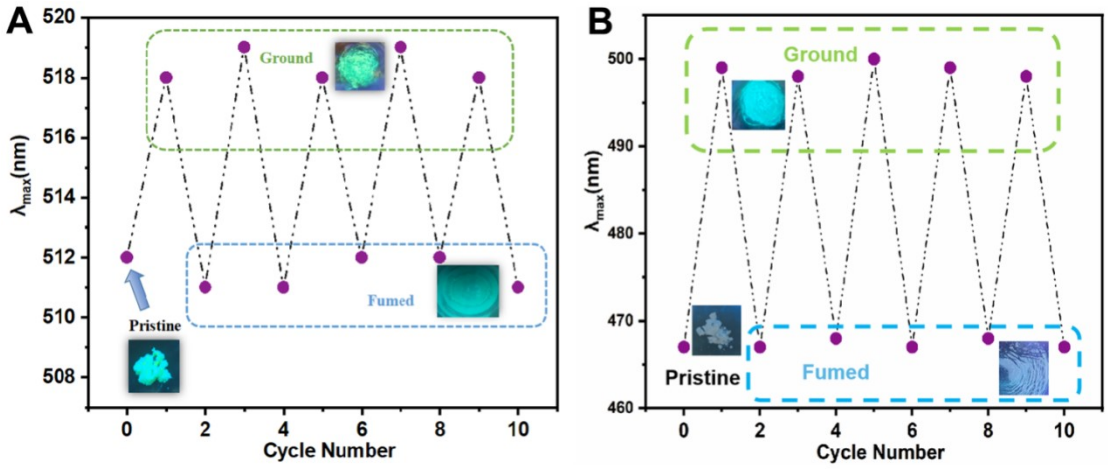

Figure S34. Reversible switching emission of pristine powder of **1-PyBP** (A) and **2-PyBP** (B) by repeating grinding–fuming cycles.

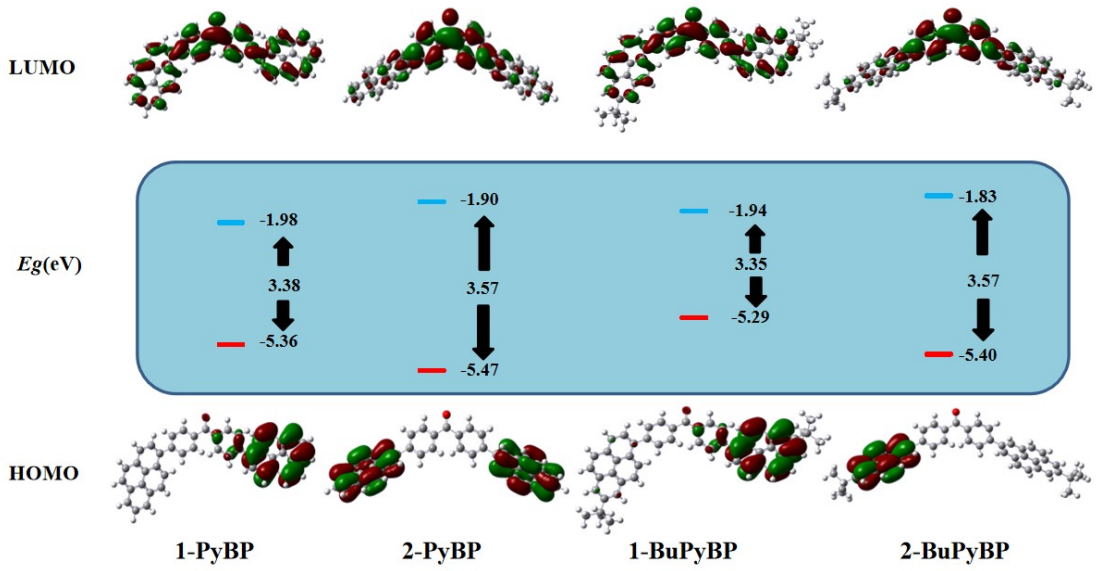

Figure S35. Frontier-molecular-orbital distributions and energy level diagrams for **1-PyBP**, **2-PyBP**, **1-BuPyBP**, and **2-BuPyBP** by DFT calculations.